Multielectron X-Ray Photoexcitation Observations in X-Ray-Absorption Fine-Structure Background

Guoguang Li, Frank Bridges, and George S. Brown
Physics Department, University of California, Santa Cruz, California 95064
(Received 4 October 1991)

Multielectron excitations involving deep and shallow core levels have been identified for the first time in the x-ray-absorption fine-structure (XAFS) energy range for crystalline samples, RbBr and β-PbO_2. The XAFS oscillations have been fitted and subtracted from the experimental data using theoretical standards. The positions of steps in the extracted background are in excellent agreement with the $Z+1$ approximation. The ability to determine this structure has important implications for XAFS and multiexcitation studies.

PACS numbers: 78.70.Dm, 32.30.Rj, 32.80.Fb, 61.10.Lx

Multielectron excitations in the x-ray absorption above K and L edges have been studied for a number of systems [1–11] and are important probes of the internal structure of the atoms. It is well known that such processes contribute significantly to the near-edge structure in absorption spectroscopy (often referred to as shake-up or shake-off processes), in the range 0–50 eV above an absorption edge. It is, however, less well known that multielectron features can exist at energies far above the edge, although they have been identified in a few special cases [1–10]. In particular they occur in the energy range 50 to approximately 1000 eV [6–10], the energy range commonly known as the XAFS (x-ray-absorption fine structure) region. In the XAFS data analysis, the XAFS oscillations are usually extracted assuming that the background is a smooth function that can be well approximated by an nth-order polynomial (n, typically 4–8) or a multiple-spline (3–6 splines) fit. When small steps occur in the background, they introduce errors [6–10] in the XAFS oscillations extracted following this standard procedure.

Recently, to obtain good fits to Pb and Bi L_{III}-edge XAFS data [12], we have developed an iterative procedure to determine the background. This procedure makes use of the new theoretical standard functions computed using the program FEFF, developed by Rehr and co-workers [13]. For the L_{III} edge of Pb and Bi, a clear, broad step is present in the background above the edge. We have now extended that analysis slightly to remove most of the XAFS structure in the absorption-edge data so that the multielectron features are more clearly revealed. For all the edges studied below, we compare the position of the step to that predicted by the $Z+1$ model [14], which appears to work well for deep atomic levels [2,6,8,9].

The x-ray-absorption data were collected on the wiggler beam line IV-1 at the Stanford Synchrotron Radiation Laboratory using Si(220) monochromator crystals, detuned 50% to reduce the harmonic content. The XAFS samples were prepared by brushing a fine powder (30 μm) onto Scotch tape. Several layers were stacked to obtain a sample with a thickness of approximately two absorption lengths. Data were collected at 80 K. For the Kr-gas K-edge study, the Dewar was filled with Kr gas at atmospheric pressure (path length $\sim$3 cm) and measurements were taken at room temperature.

To extract an accurate background function requires good XAFS standards. The comparisons between the experimental standards that we have extracted for a single atom pair and the FEFF results show that they agree very well. Figure 1 shows the Cu-Cu atom pair in wave-vector (k) space as an example. Since the theoretical XAFS calculations do not have a background problem and extend down to the low k range, these results will be used to extract the XAFS background.

Generally, we reduce and analyze the XAFS data in the following way [15]. First, a polynomial fit to the preedge data is subtracted from the entire data set. Then the background above the edge is fitted with a series of splines and the XAFS function $\chi(E)$ is obtained by the equation $\chi(E)=[\mu(E)-\mu_0(E)]/\mu_0(E)$, where the absorption cross section $\mu(E)$ includes both the absorption edge and the XAFS oscillations, and $\mu_0(E)$ (above the edge) is the free atomic absorptance, simulated here to lowest order by the spline fit. Next, $\chi(E)$ is converted to k space, using $k=[2m(E-E_0)]^{1/2}/\hbar$, where E_0 is the energy at one-half the absorption-edge height. Hence, we

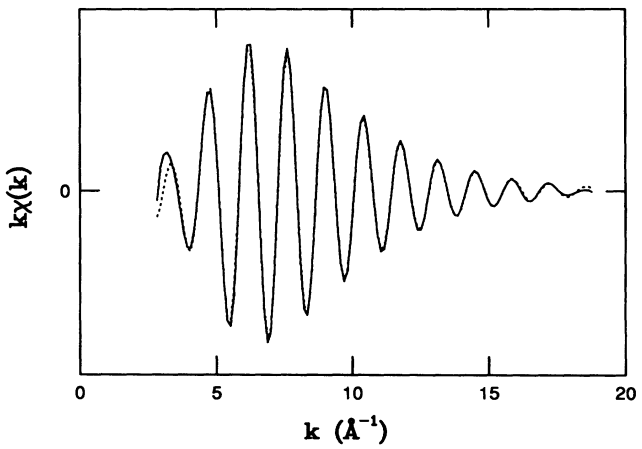

FIG. 1. A comparison of the XAFS function $k\chi(k)$ between the experimental (solid line) and theoretical (dotted line) standard for Cu-Cu atom pair. The experimental standard was extracted from Cu K-edge data of Cu foil.

extract the modulation function $k\chi(k)$ given by [15]

$$k\chi(k)=\sum_j \frac{N_j F_j(k)}{R_j^2}\sin[2kR_j+\phi_j(k)] \times\exp(-2k^2\sigma_j^2-2R_j/\lambda)\,, \quad (1)$$

where the sum is taken over shells with N_j atoms at a distance R_j from the absorbing atom, F_j is the backscattering amplitude, dependent on the kind of atom in shell j, $\phi_j(k)$ is a phase shift depending upon both the backscattering and absorbing atoms, λ is the effective electron mean free path, and σ_j^2 is the mean-square fluctuation of R_j. Finally, $k\chi(k)$ is Fourier transformed into real (r) space, using as long a k interval as possible. To obtain numerical values for R_j, N_j, and σ_j, we perform iterated least-squares fits to the real and imaginary parts of the Fourier transform of $k\chi(k)$ in a fixed range of r with identical k-space-transformed standards. In these fits in r space, the overlaps of the radial distributions of neighbors are included.

To remove the XAFS oscillations from $\mu(E)$, we first process the data in the usual way as described above. Then, the fit results in r space are transformed back to k space and energy (E) space. The XAFS background $\mu_0'(E)$ is then obtained from the equation

$$\mu_0'(E)=\mu(E)/[1+\chi_c(E)]\,, \quad (2)$$

where $\mu(E)$ is the experimental data and $\chi_c(E)$ is the calculated fit to the XAFS data, i.e., a sum of FEFF results with the fit parameters N_j, R_j, σ_j, and ΔE_{0j} (edge shift). The better the fit of $\chi_c(E)$ to the data, the smoother the extracted XAFS background $\mu_0'(E)$ will be. Next, the new background is determined by using a multiple-spline fit to this $\mu_0'(E)$ [instead of $\mu(E)$] and the whole procedure is repeated. In this way, a background function $\mu_0'(E)$ relatively free of noise (but containing a non-XAFS low-frequency signal) is obtained. We note that the Fourier transform of $k\chi(k)$ extracted by using this new background has a much better shape in the low r region than that obtained in the usual way.

We present β-PbO_2 as an example. First we reduce the experimental data in the usual way. Figure 2(a) shows the experimental data and fit results in k space. The fitting range in r space is from 1.3 to 3.9 Å. There is additional structure for r less than 1 Å in the r-space experimental data and the standards do not fit the experimental data in that region. Similar problems are found in k space for k less than 6 $Å^{-1}$ as shown in Fig. 2(a). These results indicate that a simple function does not fit the background well in the low-energy region, as was also found for a-Si:H [8]. The new background obtained from $\mu_0'(E)$ [instead of $\mu(E)$] results in a better extraction of $k\chi(k)$ and better fit results in k space [Fig. 2(b)]. The extracted background $\mu_0'(E)$ is shown in Fig. 3 (curve a). A step is visible in this background even though it is noisy because the high-r-region XAFS peaks

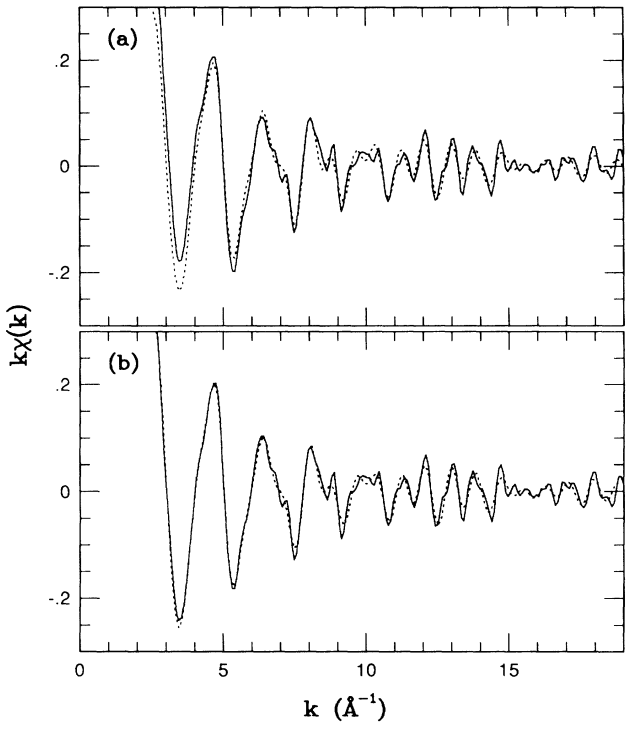

FIG. 2. The XAFS function $k\chi(k)$ of the Pb L_{III} edge for β-PbO_2. The solid lines show the experimental data reduced (a) in the usual way and (b) in the new way as described in the text. The dotted lines are the back Fourier transformation of the r-space-fit results. Only peaks for $r<4$ Å are included in the fit process; consequently there are small differences between the calculated and experimental curves, which arise from the high-frequency oscillations in the data due to more distant neighbors.

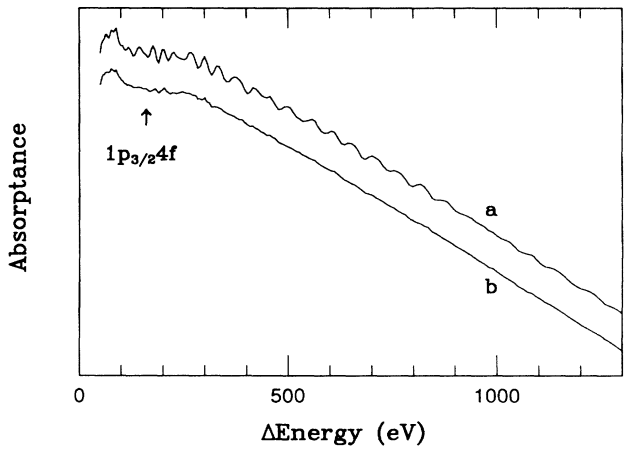

FIG. 3. The extracted XAFS background for the Pb L_{III} edge. Curve a shows the background obtained from Fig. 2(b) with the high-frequency XAFS contributions present. Curve b shows the background with the high-frequency XAFS signal removed. The curves are vertically displaced and the energy is relative to the Pb L_{III} edge. The arrow indicates the energy position predicted by the $Z+1$ model.

have not been removed.

To remove the high-frequency oscillations from the extracted XAFS background, the high-r-range data ($r > 4$ Å) were Fourier transformed back to E space [these oscillations are insensitive to the background used to extract $\chi(k)$] and then subtracted from the extracted XAFS background. The final result for the Pb L_{III} edge is shown in Fig. 3 (curve b). The step shown in the extracted background is 163 ± 5 eV above the L_{III} edge. The $Z+1$ model [14], i.e., using the x-ray atomic-energy level [16] of Bi to calculate the energy of the second core hole, gives 161.9 ± 0.5 eV and 157.4 ± 0.6 eV for the N_{VI} and N_{VII} levels, respectively. Therefore, it is clear that the step corresponds to a $1p_{3/2}4f_{5/2}(4f_{7/2})$ double-electron ionization. Here $4f_{5/2}$ and $4f_{7/2}$ cannot be resolved. A similar result is also found at the Bi L_{III} edge for a $BaBiO_3$ sample.

To compare our extracted results more directly with the experiment, we have collected Br, Kr, and Rb x-ray-absorption K-edge data using Kr gas and RbBr crystalline powder. The experimental spectrum for Kr, after preedge subtraction, is very similar to previous results [2,6]. The extracted XAFS backgrounds for Br and Rb are shown in Fig. 4 together with the Kr data for comparison. The energy positions predicted by the $Z+1$ model [14,16] are indicated by arrows. The positions of the $1s3d$ feature are in excellent agreement with the predictions of the $Z+1$ model as listed in Table I. The slopes of the three traces change in a similar way near the $1s3d$ steps. The amplitude of the double excitation for Br and Rb appears to be comparable to the corresponding Kr step, $(5.6 \pm 0.4) \times 10^{-3} \sigma_K$, but further measurements are needed to obtain exact results. The $1s4s$ excitation of Rb is also visible even though it is not well defined, partly because it is very close to (37 eV above) the K edge. Similar results are also obtained for the Br K edge from a

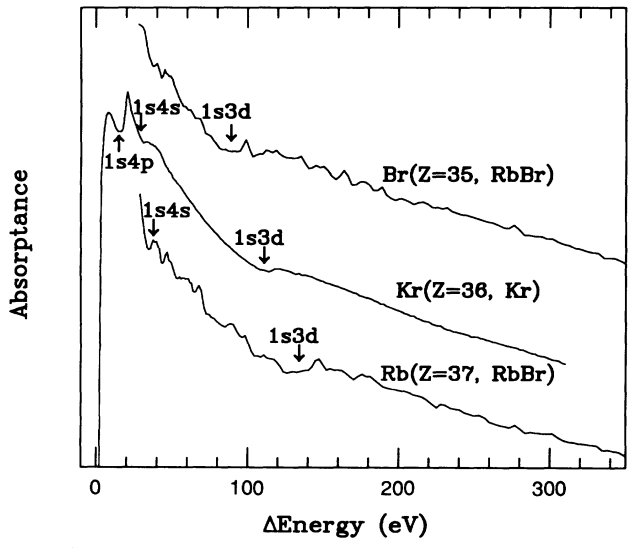

FIG. 4. The extracted XAFS background for the Br, Kr, and Rb K edges. The curves are vertically displaced. The energy is relative to the K edge of the absorbing atom and the arrows indicate the energy position predicted by the $Z+1$ model. (The step height for the $1s3d$ feature of Kr is about 0.56% of the main edge.)

TABLE I. Core holes and energies of two-electron transitions for Br, Kr, and Rb atoms. Δ energy is relative to the K edge of the absorbing atom.

Absorbing atom	Core holes	Δ energy (eV) Measurement	$Z+1$
Br($Z=35$)	$1s3d$	90 ± 5	88.9 ± 0.8
Kr($Z=36$)	$1s3d$	110 ± 2	110.3 ± 0.3
			111.8 ± 0.3
Rb($Z=37$)	$1s3d$	136 ± 5	133.1 ± 0.3
			135.0 ± 0.3

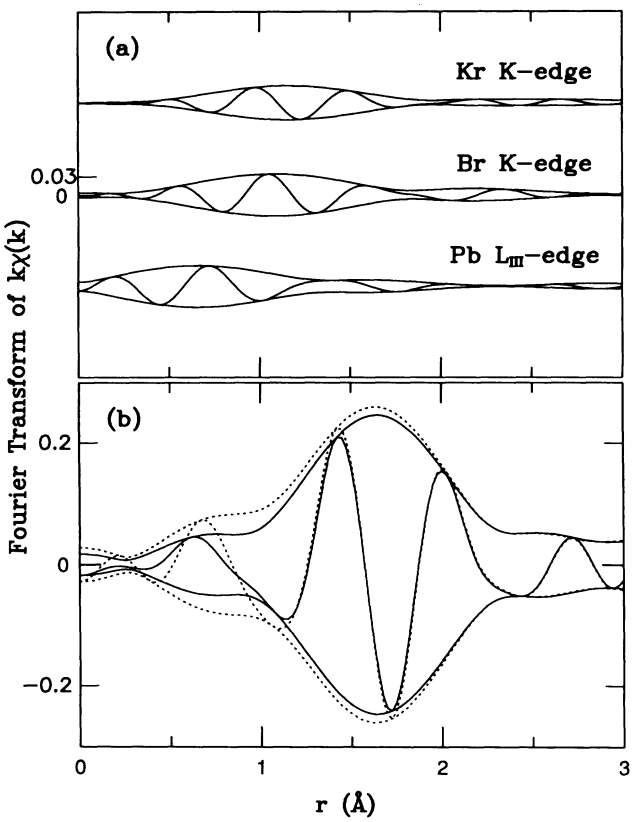

FIG. 5. (a) The Fourier transform of the function obtained from the *extracted* XAFS background for Br, Kr, and Pb in Figs. 3 and 4 using a standard XAFS data-reduction procedure with a smooth background. (b) The Fourier transform of the Pb L_{III} edge for β-PbO_2 with (dotted lines) and without (solid lines) the multielectron excitation step. The Fourier transform range is 3.5–8.0 Å^{-1}, Gaussian broadened by 0.3 Å^{-1}. The envelope curves are the magnitude of the complex transform $\pm (R^2+I^2)^{1/2}$ and the oscillatory curves are the real part of the transform.

CuBr sample.

What are the main implications of these results?

(1) For XAFS studies of systems with short bond lengths (<2.3 Å), it is important to remove multielectron excitations, if they exist in the range 30–300 eV above the absorption edge. The additional structure in the XAFS region if the multielectron features are not removed shows up at low r [see Fig. 5(a)]; it distorts and asymmetrically broadens the first peak as shown in Fig. 5(b). For investigations of anharmonicity in the first peak [17] or where this peak is the sum of two closely spaced peaks [12], it is crucial to remove these multielectron features. For highly disordered material, corrections are also needed for the XAFS if multiexcitations occur [8,10].

(2) The removal of the XAFS oscillations enables investigators to probe multielectron features over the entire energy range in solids including both the XAFS and x-ray-absorption near-edge structure (XANES) regions. It may be most helpful in the 15–80 eV range above the edge (the region where XAFS and XANES overlap) and may provide a much cleaner determination of the amplitudes and positions of the multielectron excitation features, both of which vary with the local environment [11].

In conclusion, it is possible to observe the multielectron excitation in the XAFS oscillation energy region using good XAFS standards and a careful background extraction procedure. Our method works very well and the results are in excellent agreement with the $Z+1$ approximation. It is also clearly important to include the multiexcitation steps during the XAFS data reduction [8,10].

We thank J. B. Boyce for helpful discussions. The experiments were performed at the Stanford Synchrotron Radiation Laboratory, which is supported by the U.S. Department of Energy, Office of Basic Sciences, and the National Institutes of Health, Biotechnology Division. The work is supported in part by NSF Grant No. DMR-90-04325.

[1] B. Crasemann, J. Phys. (Paris), Colloq. **48**, C9-389 (1987); A. Kodre, S. J. Schaphorst, and B. Crasemann, in *Proceedings of the Fifteenth International Conference on X-Ray and Inner-Shell Processes, July 1990*, edited by T. A. Carlson, M. O. Krause, and S. T. Manson, AIP Conf. Proc. No. 215 (AIP, New York, 1990), p. 582; B. Crasemann, in Proceedings of the Seventeenth International Conference on the Physics of Electronic and Atomic Collisions (to be published).

[2] M. Deutsch and M. Hart, Phys. Rev. A **29**, 2946 (1984); M. Deutsch, M. Hart, and P. Durham, J. Phys. B **17**, L395 (1984); M. Deutsch and M. Hart, Phys. Rev. Lett. **57**, 1566 (1986); Phys. Rev. A **34**, 5168 (1986); M. Deutsch, G. Brill, and P. Kizler, Phys. Rev. A **43**, 2591 (1991).

[3] S. I. Salem, B. Dev, and P. L. Lee, Phys. Rev. A **22**, 2679 (1980); S. I. Salem, A. Kumar, and P. L. Lee, Phys. Rev. A **25**, 2069 (1982).

[4] G. B. Armen, T. Åberg, K. R. Karim, J. C. Levin, B. Crasemann, G. Brown, M. Chen, and G. Ice, Phys. Rev. Lett. **54**, 182 (1985).

[5] M. H. Tuilier, D. Laporte, and J. M. Esteva, Phys. Rev. A **26**, 372 (1982).

[6] E. Bernieri and E. Burattini, Phys. Rev. A **35**, 3322 (1987).

[7] A. G. Kochur, A. M. Nadolinsky, and V. F. Demekhin, J. Phys. (Paris), Colloq. **47**, C8-83 (1986).

[8] A. Filipponi, E. Bernieri, and S. Mobilio, Phys. Rev. B **38**, 3298 (1988).

[9] S. Bodeur, P. Millié, E. L. á Lugrin, I. Nenner, A. Filipponi, F. Boscherini, and S. Mobilio, Phys. Rev. A **39**, 5075 (1989).

[10] K. Zhang, E. A. Stern, J. J. Rehr, and F. Ellis, Phys. Rev. B **44**, 2030 (1991).

[11] A. Bianconi, J. Garcia, M. Benfatto, A. Marcelli, C. Natoli, and M. Ruiz-Lopez, Phys. Rev. B **43**, 6885 (1991).

[12] J. B. Boyce, F. G. Bridges, T. Claeson, T. H. Geballe, G. G. Li, and A. W. Sleight, Phys. Rev. B **44**, 6961 (1991).

[13] J. Mustre de Leon, J. J. Rehr, S. I. Zabinsky, and R. C. Albers, Phys. Rev. B **44**, 4146 (1991).

[14] J. Briand, A. Touati, M. Frilley, P. Chevallier, A. Johnson, J. P. Rozet, M. Tavernier, S. Shapoth, and M. O. Krause, J. Phys. B **9**, 1055 (1976).

[15] T. M. Hayes and J. B. Boyce, in *Solid State Physics*, edited by H. Ehrenreich, F. Seitz, and D. Turnbull (Academic, New York, 1982), Vol. 37, p. 173.

[16] *Handbook of Chemistry and Physics*, edited by R. C. Weast (CRC, Boca Raton, Florida, 1989), p. E-191.

[17] J. Mustre de Leon, S. D. Conradson, I. Batistić, and A. R. Bishop, Phys. Rev. Lett. **65**, 1675 (1990); Phys. Rev. B **44**, 2422 (1991).